New Thermo-Physical Modeling of EDM with The Latent Heat Consumption

Tomoki Iwata

Technology Development Section, FB Co., Ltd., Japan

Abstract:- The electrical discharge machining (EDM) is a thermal process which machines electrical conductive materials, irrespective of its hardness. The temperature of the plasma that is ignited between the tool electrode and the workpiece reaches several thousand degrees, and the plasma power is distributed to the tool electrode, the workpiece and the dielectric fluid.

Finding out the power fraction to the workpiece is quite important to improve the performance of EDM, and the transient heat conduction analysis is necessary to determine the power fraction to the workpiece. For the accurate analysis, temperature dependence of thermo-physical properties of the material and the latent heat of the material ought to be included in a thermo-physical model of the analysis.

In this study, a new algorithm that computes the latent heat consumption at the certain temperature was developed and included into the thermo-physical model. The transient heat conduction analyses were carried out using the model. Consequently, the power fraction to the workpiece was determined by comparing the computing results and the experimental results.

The melt volume computed with the conventional latent heat incorporated model and the melt volume computed with the no latent heat model were discussed as well.

Keywords:- EDM, Latent heat, Heat flux, Plasma radius, Power fraction

I. INTRODUCTION

Electrical discharge machining (EDM) is one of the most useful machining methods to cut hard material and widely used especially in a mold manufacturing field. EDM is a thermal process. The thermal energy is created by repeated pulse discharges generated between the tool electrode and the workpiece. In EDM, the electrodes (the tool electrode and the workpiece) are submerged in dielectric oil usually.

The machining process in EDM consists of two important processes. On is a melting process of the workpiece, and the other is a removal process of the melting portion of the workpiece. In the melting process, the workpiece material is melted by means of the heat flux from thermal plasma generated between electrodes. On the other hand, in the removal process, a portion of the melted workpiece is removed by the effect of the superheating mainly [1,2]. Since not melted portion of the workpiece can not leave the workpiece body, the melting process in EDM is extremely important.

In the melting process, a certain fraction of plasma power goes into the workpiece surface as a heat flux, and it raises the workpiece temperature. The stored heat at the workpiece surface is transferred inside the workpiece body by means of conduction. To find the power fraction to the workpiece, the transient heat conduction analysis inside the workpiece is necessary. For the analysis, the value of latent heat of the workpiece material is required as well as the thermo-physical property of the workpiece material. Studies [3-6] have incorporated the latent heat into the computing model. In this conventional model, the amount of latent heat of melting is distributed over the temperature range from the room temperature to the melting point. However, the conventional model does not completely express an actual latent heat consumption phenomenon faithfully.

In this study, the author examined a new thermo-physical model that represents the latent heat consumption phenomenon more faithfully and carried out the transient heat conduction analysis using the new model to compute the amount of melt volume of the workpiece. After the computation, the power fraction to the workpiece was estimated by comparing the computed melt volume with the experimental melt volume.

II. LATENT HEAT ALGOLITHM

In the melting process of EDM, the latent heat of melting means an amount of heat consumed by the workpiece body at the melting point of the material for the phase change without any temperature rising. In the literatures [3-6], the latent heat of melting is considered to be distributed over the temperature range from room temperature to the melting point of the workpiece material, and the amount of latent heat is incorporated into the specific heat of the material. For example, the effective heat capacity C_{peff}, which is the latent heat distributed specific heat, is defined as Eq. (1) in the literature [3];

$$C_{Peff} = C_P + \frac{L_h}{\Delta T} \tag{1}$$

where C_p is specific heat, L_h is latent heat and ΔT is the temperature range from room temperature to the melting point. However, the actual meaning of the latent heat of melting is an amount of heat consumed for the phase change from the solid to the liquid at the melting point without any temperature rising. Therefore, Eq. (1) which is distributing the latent heat over the temperature range ΔT does not agree this latent heat meaning. Moreover, the effective heat capacity C_{peff} given by Eq. (1) is quite different from the original temperature dependency of specific heat property of the material. Consequently, the results of heat conduction analysis using Eq. (1) lack accuracy.

Accordingly, the author developed a new algorithm that simulates the latent heat consumption at the melting point without any temperature rising of the workpiece, and included the algorithm into the thermo-physical model. Fig. 1 shows the latent heat consumption algorithm. In Fig. 1, L_m is the latent heat and T_m is the melting point. In the algorithm, if the temperature T_n for calculating step n is more than T_m and the temperature T_{n-1} for the previous step n-1 is not exceeding T_m, then L_m' is calculated by Eq. (2). When L_m' is zero or more, L_m is replaced with L_m' and T_n is replaced with T_m. If L_m' is a negative number, the sign of L_m' is reversed and L_m is replaced with L_m'; then T_n is recalculated by Eq. (3).
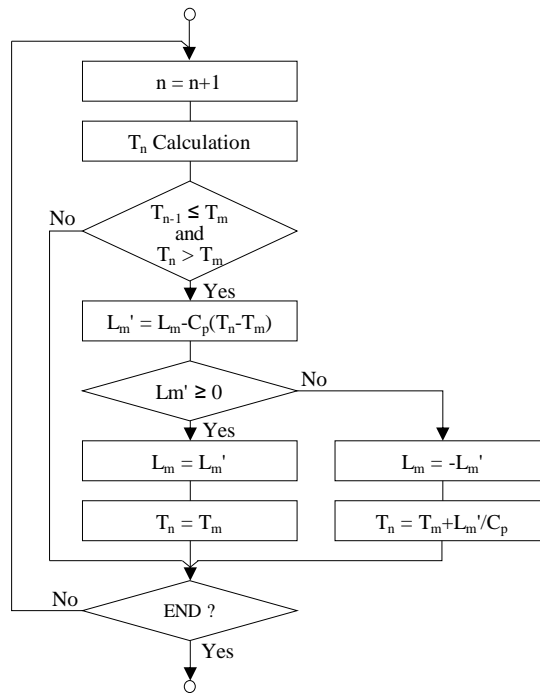
Fig. 1: The algorithm of latent heat consumption

$$L'_m = L_m - C_P(T_n - T_m) \tag{2}$$

$$T_n = T_m + \frac{L'_m}{C_P} \tag{3}$$

This algorithm procedure is repeated until the discharge duration has been passed. Following the calculating procedure shown in Fig. 1, the consumption of latent heat of melting is well simulated. The consumption of latent heat of vaporization is also incorporated into the thermo-physical model.

III.   ASUMPTIONS

A. Heat Flux Distribution

The total power generated by thermal plasma is distributed to the workpiece, the tool electrode and the dielectric oil. The total power is given by;

$$P_A = P_W + P_T + P_D \tag{4}$$

where P_A is a total power, P_W is a power distributed to the workpiece, P_T is a power distributed to the tool electrode and P_D is a power distributed to the dielectric oil. The fraction of power to the workpiece is given by;

$$F_W = \frac{P_W}{P_A} \tag{5}$$

where F_W is the fraction of power to the workpiece. The power P_W is transferred to the workpiece surface by a heat flux which is given by;

$$Q_W = \frac{P_W}{A_W} = \frac{IVF_W}{A_W} = \frac{IVF_W}{\pi R_h^2} \tag{6}$$

where Q_W is the heat flux to the workpiece, A_W is an area of the workpiece surface where the heat flux enters, I is a discharge current, V is a discharge voltage and R_h is a heat input radius.

Researchers have proposed three forms of heat flux distribution on the workpiece surface, namely point heat source model with hemispherical crater cavity [7], uniformly distributed heat flux model [8] and Gaussian distribution heat flux model [9]. In these three models, the Gaussian distribution heat flux model is more consistent with the actual EDM case [10]. Therefore, the Gaussian distribution heat flux model was used in this study. The Gaussian distribution heat flux is given by Eq. (7) and Eq. (8) [9];

$$Q(r) = Q_0 \exp\left\{ -4.5\left(\frac{r}{R_h}\right)^2 \right\} \tag{7}$$

$$Q_0 = 4.57\frac{IVF_W}{\pi R_h^2} \tag{8}$$

where r is a coordinate in radial direction and Q_0 is the maximum heat flux at r=0.

B. Plasma Radius

Researchers [5,11] reported that the plasma radius expands with the passage of discharge time. However, the comprehensive equation that expresses the expanding plasma radius algebraically has not been found.

Ikai et al. [12] proposed non-expanding plasma which has the same melting ability as actual expanding plasma. This non-expanding plasma radius is termed as "equivalent heat input radius" and is given by [12];

$$R_{eq} = (2.04E - 03)I^{0.43} \cdot t_{on}{}^{0.44} \qquad (\mu m) \tag{9}$$

where R_{eq} is the equivalent heat input radius, I is discharge current and t_{on} is discharge duration. However, there are two questions about the equivalent heat input radius. One question is that the model of equivalent heat input radius consists of uniform distribution of heat intensity, and R_{eq} is the same as the crater radius. The outer side area of the heat flux seems to have an insufficient intensity to melt the workpiece since the actual heat flux has the Gaussian distribution as Eq. (7). Therefore, the actual heat input radius is considered to be greater than the crater radius. The other question is that R_{eq} was determined by the experiments using a needle shaped tool electrode and flat plane shaped workpiece. In usual EDM process, as the transcription shape of tool electrode is machined on the workpiece, the tool electrode surface and the workpiece surface are considered to be parallel. In the case of needle shaped electrode is used, the electrical field and the flow behavior of dielectric oil between electrodes are much different from the usual EDM.

In this study, the author introduced the Gaussian distribution heat flux with a fixed radius. The radius is termed as "effective radius of heat input (R_{eff})" which has the same melting ability as actual expanding plasma. The effective radius of heat input is larger than the actual crater radius. Fig. 2 shows an image of the heat flux employed for the transient heat conduction analysis in this study.
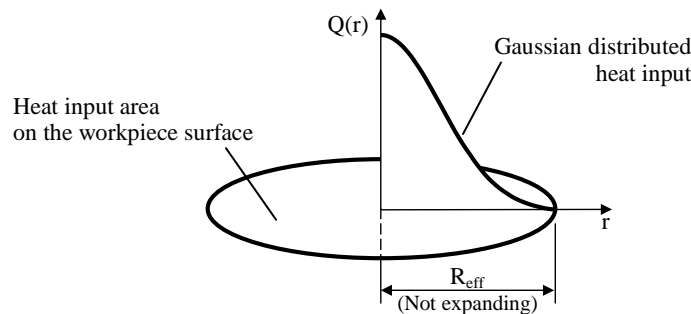
Fig. 2: The image of the heat flux to the workpiece

C. Thermo-physical Properties

The temperature dependency of thermo-physical properties of the workpiece material (0.45%C carbon steel, JIS-S45C) has not been cleared. Therefore, the properties of iron were used in this study. Table I shows the thermo-physical properties of iron and Table II shows the latent heat of iron.

Table I: Thermo-physical Properties of Iron

Temperature [K]	Density [kg/m³]	Specific heat [J/(kg·K)]	Thermal conductivity [W/(m·K)]
250	7880	422	86.5
300	7870	442	80.3
600	7770	566	54.7
800	7700	686	43.3
1000	7620	1030	32.6
1200	7630	600	28.2
1811	7035	795	40.3

Table II: Latent Heat of Iron

Temperature [K]	Latent heat [J/kg]
1811 (Melting point)	2.47E+05
3136 (Boiling point)	6.34E+6

IV. COMPUTING MODEL AND GOVERNING EQUATION

The axisymmetric cylindrical coordinates were applied to the transient heat conduction analysis of the workpiece because the heat input to the workpiece is circle shaped as shown in Fig. 2. Fig. 3 shows the schematic representation of the computation model.
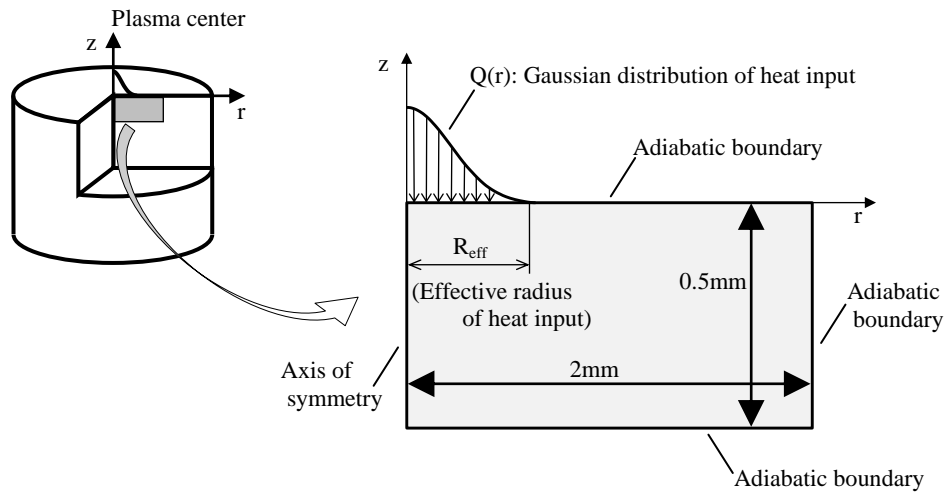
Fig. 3: The computation model of the workpiece

For the axisymmetric cylindrical coordinate system, the governing equation is given by;

$$C_P \rho \frac{\partial T}{\partial t} = \frac{1}{r} \frac{\partial}{\partial r}\left(r\lambda \frac{\partial T}{\partial r} \right) + \frac{\partial}{\partial z}\left(\lambda \frac{\partial T}{\partial z} \right) \tag{10}$$

where r and z are the coordinates, T is temperature, λ is thermal conductivity, ρ is density and C_P is specific heat. The computing conditions are shown in Table III. The temperature of each element was calculated by the method of finite differences.

Table III: Computing Conditions

| Item	Value
Lattice point distance (Δr)	1μm
Lattice point distance (Δz)	1μm
Time step (Δt)	10ns
Discharge current (I)	10A
Discharge voltage (V)	22V
Discharge duration	250μs
Initial temperature	296K
Effective radius of heat input (R_{eff})	20 - 400μm
Power fraction to the workpiece (F_W)	5 - 18.3%

V. RESULTS OF THE ANALYSIS

Fig. 4 shows an example of the temperature distribution around the discharge point of the workpiece. Fig. 5, Fig. 6 and Fig. 7 show the computing results. Fig. 5 shows the relationship between R_{eff} and melt volume per pulse. Fig. 6 shows the relationship between R_{eff} and melt radius. Fig. 7 shows the relationship between R_{eff}

and maximum melt depth. In Fig. 5, the melt volume per pulse has the maximum value. The melt volume increases with the increase of R_{eff} until the melt volume reaches the maximum value. The melt radius also has the maximum value in Fig. 6. Fig. 7 indicates that the melt depth decreases with the increase of R_{eff} without any extreme value. Too large R_{eff} that exceeds a certain value makes melt volume and melt radius smaller due to a reduction in the heat flux that is less than the melt enough power.
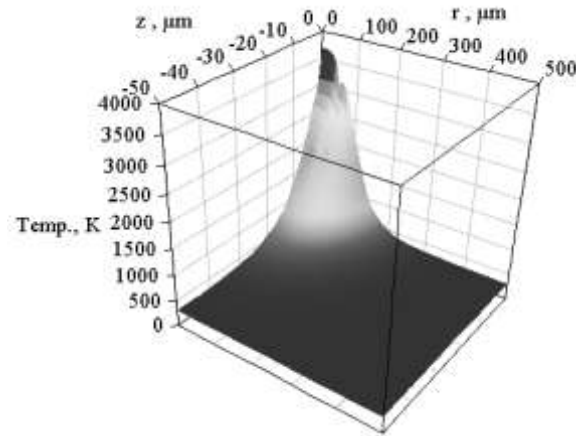
Fig. 4: Example of temperature distribution of the workpiece
(In the case of effective radius of heat input is 200µm and power fraction is 14%)
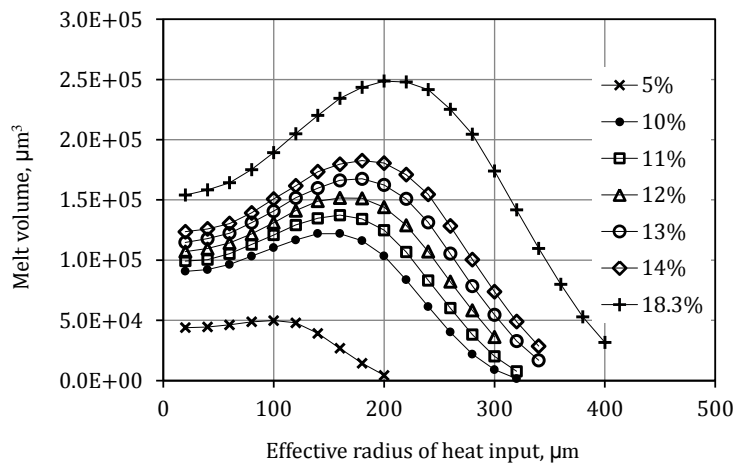
Fig. 5: Relationship between effective radius of heat input
and calculated melt volume per pulse of the workpiece
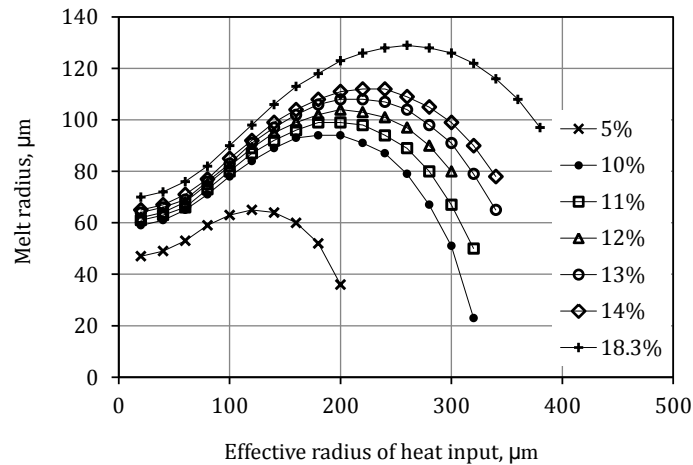
Fig. 6: Relationship between effective radius of heat input
and calculated melt radius at the workpiece top surface
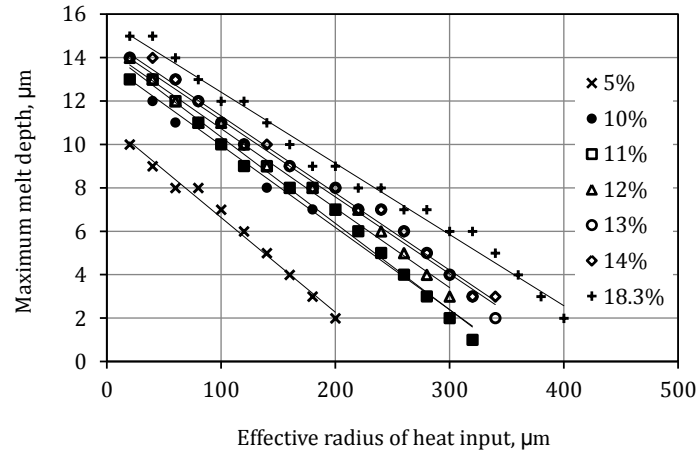
Fig. 7: Relationship between effective radius of heat input
and calculated maximum melt depth of the workpiece

VI.   RESULTS OF EXPERIMENTS

In this section, the melt volume per pulse and the melt radius were found from the experimental results to compare the computing results.

A. Melt Volume

The author and Hirose [13] carried out EDM experiments using nine types of dielectric oil. The experiments were performed on a die sinking EDM machine (SODICK AQ35L). The machining conditions are shown in Table IV, and the results of workpiece removal mass (mg/4min.) are shown in Fig. 8. Fig. 8 shows that the removal mass vary with the oil type. In Fig. 8, oil A, oil G and oil I show the minimum, the intermediate and the maximum removal mass respectively. The total removal volume is calculated by dividing the removal mass by the material density. The calculated removal volume is a part of whole melt volume of the workpiece during the machining. The rest of the whole melt volume of workpiece is remaining at the workpiece surface as a white layer.

Table IV: Machining Conditions of the Experiments

| Item	Description
Tool electrode material	Copper
Workpiece material	0.45%C carbon steel
Machined area	9mm×5mm
Open circuit voltage	90V
Servo reference voltage	40V
Discharge current	10A
Discharge duration	250μs
Pulse interval	250μs
Workpiece polarity	Cathode
Machining time	4min.
Dielectric oil	9types (A – I)
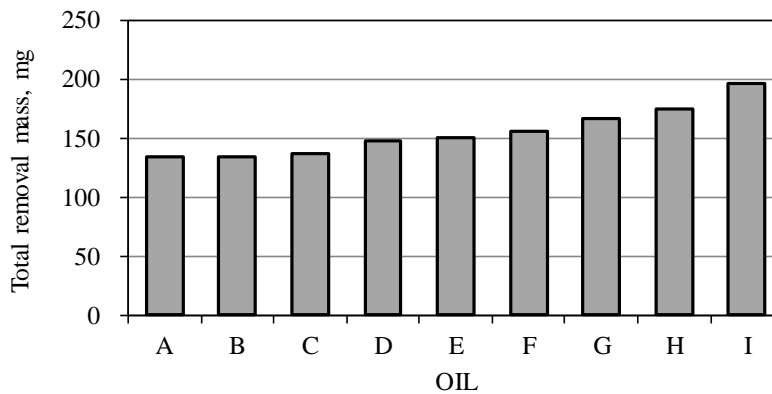
Fig. 8: Total removal mass of the workpiece for 4min. machining

Fig. 9 is an example of cross-section view of EDMed workpiece. To observe the cross-section clearly, the cross section was well polished and etched with nital. Fig. 9 shows the white layer that is re-solidified on the workpiece surface after being melted once. The whole melt volume during EDM is calculated by adding the total removal volume and the white layer volume. The melt volume per pulse is calculated by dividing the whole melt volume by the number of discharges.

The average white layer thickness was measured by the cross-section observation, and the white layer volume is calculated by multiplying the average thickness by machined surface area ($45mm^2$) [13]. The melt volume per pulse is given by;

$$V_{melt} = \frac{V_{WL} + V_{remv}}{N} \tag{11}$$

where V_{melt} is the melt volume per pulse, V_{WL} is the white layer volume, V_{remv} is the removal volume and N is a number of discharges. As a results of experiments, the melt volume per pulse of oil A, oil G and oil I were $7.59E+04\mu m^3$, $9.17E+04\mu m^3$ and $11.18E+04\mu m^3$ respectively.
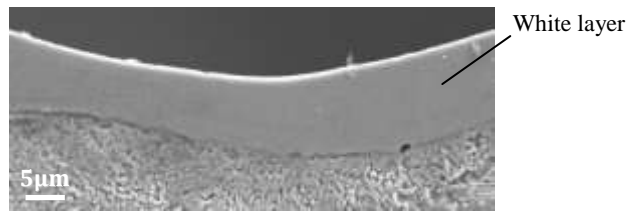

Fig. 9: Example of white layer observation

B. Melt Radius

In literatures [5,11,12], the melt radius is determined by the single pulse discharge using needle shaped tool electrode. However, in usual EDM, as the transcription shape of the tool electrode is machined on the workpiece, the tool electrode surface and the workpiece surface are considered to be parallel. In the case of needle shaped tool electrode is used for experiments, the electrical field between electrodes and the flow behavior of dielectric oil around the discharge point are much different from the usual EDM.

Though the melt radius should be determined by using parallel plane electrodes, to ignite single discharge between parallel planes with the gap of tens of micrometers is very difficult. Therefore, the melt radius is determined from the craters machined with the conditions shown in Table IV (not the single discharge).

Before determining the melt radius, the author observed a form of single pulse discharge crater using needle shaped tool electrode for reference. Fig. 10 shows the crater form. In Fig. 10, the bulge around the crater is re-solidified material. The re-solidified layer (white layer) exists under the crater also. Fig. 11 shows an image of single discharge crater. The diameter D_0 in Fig. 11 is the melt diameter of the crater. Seeing from right above, the diameter D_2, which traces the crest of the bulge, seems to be very close to D_0. Therefore, D_2 was accepted as the melt diameter in substitution for D_0 in this study.

Fig. 12a shows the whole EDMed surface machined with dielectric oil I. Fig. 12b shows an example of the crater which is enlargement of Fig. 12a. As shown in Fig. 12b (white dashed circle), the melt radius was found by tracing the crest of the recast bulge. Seventy melt radii were measured for each of three EDMed surfaces. Fig. 13 shows the histogram of melt radii. The average values of seventy melt radii for oil A, oil G and oil I are $96\mu m$, $99\mu m$ and $104\mu m$ respectively.
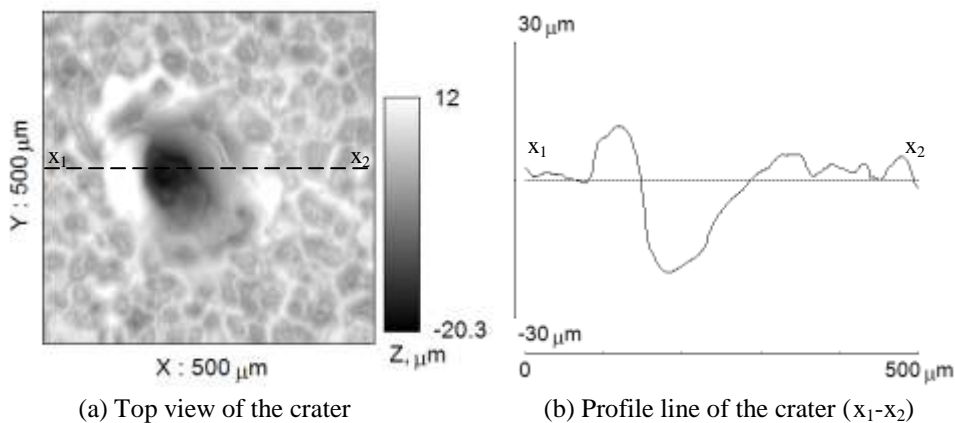
(a) Top view of the crater (b) Profile line of the crater (x_1-x_2)
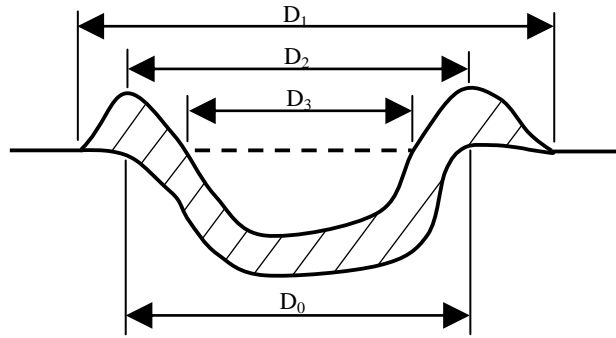**Fig. 10:** Single discharge crater

Fig. 11: Cross section image of the crater
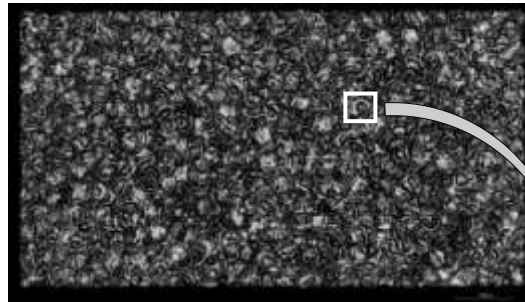

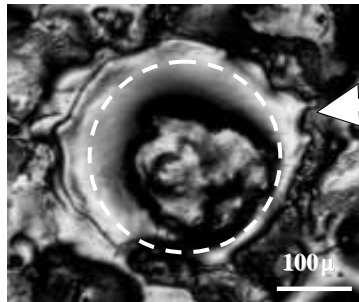**Fig. 12(a):** Whole EDMed surface and the crater

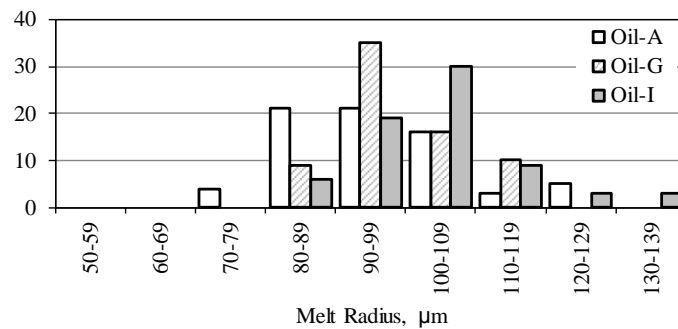**Fig. 12(b):** Enlargement of a crater

Fig. 13: Histogram of the melt radius

VII.   DISCUSSIONS

A. Power Fraction to the Workpiece

Fig. 14, which is integrated two figures of Fig. 5 and Fig. 6, shows the relationship between the melt volume per pulse and the melt radius. The experimental results of melt volume per pulse and melt radius for each oil are plotted in Fig. 14, indicating that the power fractions of oil A, oil G and oil I are 12.4%, 12.2% and 12.8% respectively.

The melt radius and the power fraction for each oil are plotted in Fig. 15, which is the enlargement of Fig. 6, indicating that the effective radii of oil A, oil G and oil I are 272μm, 255μm and 246μm respectively.
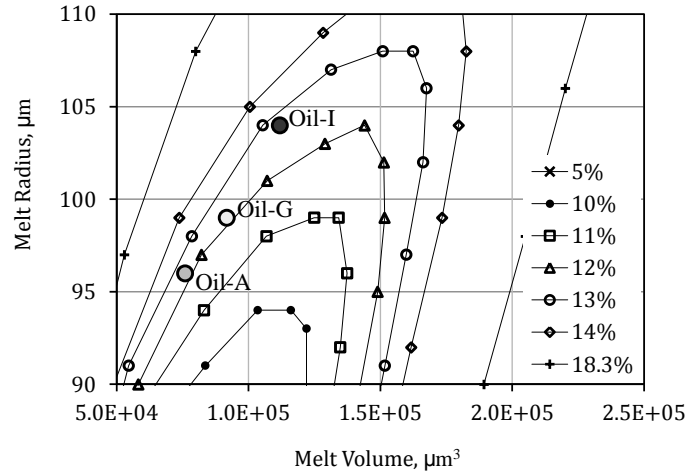
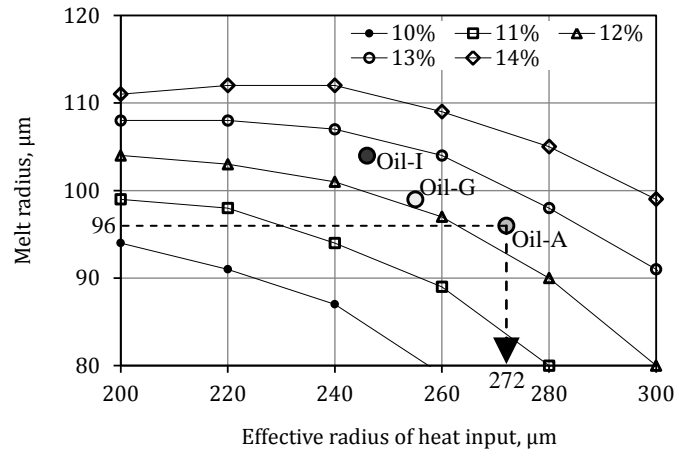**Fig. 14:** Determination of power fraction to the workpiece

Fig. 15: Determination of effective radius of heat input

B. Conventional Model and No Latent Heat Model

In the case of R_{eff} is 246μm and F_W is 12.8%, the melt volume per pulse calculated using Eq. (1) (the conventional latent heat incorporating model) is 10.46E+04μm³ while the experimental result was 11.18E+04μm³. On the other hand, the melt volume calculated with no latent heat is 13.98E+04μm³. The conventional latent heat incorporating model calculates the melt volume 6.4% smaller than the experimental result, and the no latent heat model calculates the melt volume 25% larger than the experimental result. Therefore, the modeling method of latent heat affects the calculated melt volume surely. The latent heat consumption model developed in this study is very suitable for the melting process analysis because it represents the actual latent heat consumption phenomenon faithfully.

VIII. CONCLUSIONS

In this study, the author developed a new algorithm, which simulates the latent heat consumption more faithfully, incorporating into the thermo-physical model of EDM. The transient heat conduction analysis using three types of model, such as this newly developed thermo-physical model, conventional latent heat incorporating model and no latent heat model, were carried out to compute the melt volume of the workpiece. The results indicate that the modeling method of latent heat affects the calculated melt volume.

In conclusion, the new thermo-physical model developed in this study makes the transient heat conduction analysis extremely accurate.

REFERENCES

[1]. B. N. Zolotykh, The Mechanism of Electrical Erosion of Metals in Liquid Dielectric Media, Soviet Physics-Technical Physics, Vol.4, No.12 (1959) pp.1370-1373

[2]. P. T. Eubank, M. R. Patel, M. A. Barrufet and B. Bozkurt, Theoretical models of the electrical discharge machining process III. The variable mass, cylindrical plasma model, Journal of Applied Physics, Vol.73, No.11 (1993) pp.7900-7909

[3]. S. N. Joshi, S. S. Pande, Thermo-physical modeling of die-sinking EDM process, Journal of Manufacturing Process, Vol.12 (2010) pp.45-56

[4]. Harminder Singh, Experimental study of distribution of energy during EDM process for utilization in thermal models, International Journal of Heat and Mass Transfer, Vol.55 (2012) pp.5053-5064

[5]. Y. Zhang, Y. Liu, Y. Shen, Z. Li, R. Ji, B. Cai, A novel method of determining energy distribution and plasma diameter of EDM, International Journal of Heat and Mass Transfer, Vol.75, (2014) pp.425-432

[6]. S. H. Yeo, W. Kurnia, P. C. Tan, Critical assessment and numerical comparison of electro-thermal models in EDM, Journal of Materials Processing Technology, Vol.203 (2008) pp.241-251

[7]. D. D. DiBtonto, P. T. Eubank, M. R. Patel, M. A. Barrufet, Theoretical models of the electrical discharge machining process. I., A simple cathode erosion model, Journal of Applied Physics, Vol.66, No.9 (1989) pp.4095-4103

[8]. J. V. Beck, Transient temperatures in a semi-infinite cylinder heated by a disk heat source, International Journal of Heat and Mass Transfer, Vol.24 (2010) pp.1631-1640

[9]. H. K. Kansal, S. Singh, P. Kumar, Numerical simulation of powder mixed electric discharge machining (PMEDM) using finite element method, Mathematical and Computer Modeling, Vol.47 (2008) pp.1217-1237

[10]. Y. Zhang, Y. Liu, Y. Shen, Z. Li, R. Ji, F. Wang, A new method of investigation the characteristics of the heat flux of EDM plasma, Procedia CIRP, Vol.6 (2013) pp.450-455

[11]. B. Revaz, G. Witz, R. Flükiger, Properties of the plasma channel in liquid discharges inferred from cathode local temperature measurements, Journal of Applied Physics, Vol.98 (2005) 113305

[12]. T. Ikai, I. Fujita, K. Hashiguchi, Heat Input Radius for Crater Formation in the Electric Discharge Machining, Transactions of the Institute of Electrical Engineers of Japan, Vol.112-D, No.10 (1992) pp.943-949

[13]. T. Iwata, K. Hirose, Experimental Study of Material Removal Efficiency in EDM Using Various Types of Dielectric Oil, International Journal of Engineering Research and Development, Vol.11 Iss.8 (2015) pp.34-41